Journal of Power Sources 245 (2014) 529–536

Contents lists available at SciVerse ScienceDirect

Journal of Power Sources

journal homepage: www.elsevier.com/locate/jpowsour

Reduced graphene oxide with ultrahigh conductivity as carbon coating layer for high performance sulfur@reduced graphene oxide cathode

Hongbin Zhao [a,*], Zhenhuan Peng [a], Wenjun Wang [a], Xikun Chen [b], Jianhui Fang [a], Jiaqiang Xu [a,c,*]

[a] College of Science, Shanghai University, Shanghai 200444, China
[b] School of Mechatronic Engineering and Automation, Shanghai 200444, China
[c] State Key Laboratory of Transducer Technology, Shanghai Institute of Microsystem and Information Technology, Shanghai 200050, China

HIGHLIGHTS

- S@rGO composite was synthesized via HI reduction and surfactant assisted chemical method.
- The mechanism of HI reduction of GO with high conductivity is suggested.
- 980 mAh g^{-1} capacity is kept after 200 cycles charge/discharge process.
- High C-rate current activation is used to prevent the shuttle of polysulfide ions.

GRAPHICAL ABSTRACT

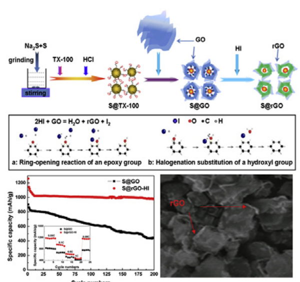

ARTICLE INFO

Article history:
Received 27 May 2013
Received in revised form
27 June 2013
Accepted 1 July 2013
Available online 9 July 2013

Keywords:
Sulfur
Cathode
Rechargeable batteries
Graphene

ABSTRACT

We developed hydrogen iodide (HI) reduction of rGO and surfactant-assisted chemical reaction- deposition method to form hybrid material of sulfur (S) encapsulated in reduced graphene oxide (rGO) sheets for rechargeable lithium batteries. The surfactant-assisted chemical reaction–deposition method strategy provides intimate contact between the S and graphene oxide. Chemical reduced rGO with high conductivity as carbon coating layer prevented the dissolution of polysulfide ions and improved the electron transfer. This novel core–shell structured S@rGO composites with high S content showed high reversible capacity, good discharge capacity retention and enhanced rate capability used as cathodes in rechargeable Li/S cells. We demonstrated here that an electrode prepared from a S@rGO with up to 85 wt% S maintains a stable discharge capacity of about 980 mAh g^{-1} at 0.05 C and 570 mAh g^{-1} at 1C after 200 cycles charge/discharge. These results emphasize the importance of rGO with high electrical conductivity after HI-reduced rGO homogeneously coating on the surface of S, therefore, effectively alleviating the shuttle phenomenon of polysulfides in organic electrolyte. Our surfactant-assisted chemical reaction-HI reduction approach should offer a new technique for the design and synthesis of battery electrodes based on highly conducting carbon materials.

1. Introduction

Lithium rechargeable cells have become one of the most important and efficient devices for storage of electrical energy and attract more attention on developing active materials. Therefore, a breakthrough in novel electrochemically active materials with high energy density is in high demand for extending their applications

* Corresponding authors. College of Science, Shanghai University, Shanghai 200444, China. Tel.: +86 21 66132406.
E-mail addresses: hongbinzhao@shu.edu.cn (H. Zhao), xujiaqiang@shu.edu.cn (J. Xu).

0378-7753/$ – see front matter © 2013 Elsevier B.V. All rights reserved.
http://dx.doi.org/10.1016/j.jpowsour.2013.07.002

to storing electricity from renewable sources [1]. One of the most attractive candidates for storage devices is the Li–S cell because of its higher theoretical specific capacity of 1672 mAh g^{-1}, corresponding to a theoretical specific energy of 2600 Wh kg^{-1} [2]. Furthermore, abundant resources, low cost and environmental friendliness are obvious advantages for its application.

However, the low electrical conductivity of sulfur and polysulfides (Li_4S_8, Li_2S_8) limits active material utilization due to poor electrochemical contacts within the material and carbon modification layer. Besides, the high dissolution of electrochemical reaction products of polysulfides (Li_2S_x, where $1 \le x \le 8$) and the redox shuttle mechanism make capacity faded quickly [2–4]. To enable operating the Li–S battery, the S cathode material must be well combined with a high conductive and a strong adsorbing agent. Various carbon materials, such as activated carbon [5], multiporous carbon [6–9] and carbon nanotubes [10–12] have been intensively investigated as additives for Li–S batteries.

Recently, graphene nanosheet (GNS), a two-dimensional structure of carbon atoms with high surface area, superior electrical conductivity, chemical stability, and mechanical properties, has attracted high attention for use of energy storage applications [13,14]. Wang et al. resorted that S was melted and coated on the GNS, which shows an improved capacity [15]. Zhang et al. [16] prepared sulfur/graphene nanosheets (S/GNS) composite through thermal reduction between the sulfur (S) and graphene oxide (GO). Wang et al. suggested a new method to synthesize a graphene–sulfur composite material by synthesizing submicrometer sulfur particles coated with PEG containing surfactants and GNS. The composite showed high specific capacity with relatively good cycling stability as the cathode for Li–S batteries [17]. Park [18] reported a practical route for synthesizing a sulfur-impregnated graphene composite as a promising cathode material for lithium–sulfur batteries with high discharge capacity.

It should be noted that GNS and GO in these methods still be insulting or partially reduced and the conductivity of S–GNS composite is low. A conjecture that a structure with reduced graphene nanosheet layer closely coating on the surface of elemental sulfur maybe is a promising strategy to improve the conductivity of S-based cathode and prevent the polysulfide ions dissolution. Several polymer materials, such as polypyrrole and polyaniline also have been researched as a support of sulfur [12,19–22]. Besides, Wang also used S-PAN and GO to obtain a compound with two different chemical state of sulfur and this novel dual-mode sulfur-based cathode material demonstrates outstanding electrochemical performances in the rechargeable Li–S batteries [23].

Herein, we reported a new likely core–shell structured Sulfur@reduced graphene composite synthesized by facile chemical method with large mass preparation and improved electrochemical cycling performance as cathode of Li–S batteries. TX-100 was used as the dispersing agent of elemental sulfur and the linker between graphene and sulfur. Hydrogen iodide was first time used to reduce graphene oxide and a core–shell structure with homogenous graphene layer coating on the surface of sulfur was fabricated successfully. Closely contact between reduced graphene and elemental sulfur supplies high conductivity of S@rGO electrode and the dissolution and shuttle of polysulfides were prevented effectively. The HI reduction provides a common route to synthesis rGO coating electrode materials, such as $LiFePO_4$, V_2O_5 and Cr_2O_3.

2. Experimental section

2.1. Synthesis

All the agents were purchased from Sinopharm Chemical Reagent Co, Ltd. China, without purification. Graphene oxide was synthesized as follows: GO was prepared by oxidizing natural flake graphite (about 300 meshes, Qingdao Tianhe Graphite Co., Ltd. China) with a procedure following traditional modified Hummers method that produced mostly several layers GO [24,25]. Briefly, the graphite was first treated with conc. H_2SO_4, P_2O_5, and $K_2S_2O_8$. After filtered and washed with DDI water for several times, the suspension was dried at 45 °C for 24 h, the pretreated graphite was obtained. The pretreated flake graphite was further oxidized to graphite oxide by three step oxidation method in ice bath, at 35 °C and 98 °C. The solid was re-suspended in conc. H_2SO_4 and further oxidized by $KMnO_4$. Afterward, 3wt % H_2O_2 was added to change residual $KMnO_4$ to Mn^{2+} in conc. H_2SO_4 solution, thus a thick and brownish yellow suspension was obtained. The graphite oxide suspension was washed with 10% HCl aqueous solution, then repeatedly with DDI (distilled, deionized) water until pH is 7, and dried at 40 °C for 24 h. Finally, graphite oxide was dispersed in DDI water with GO concentration of 1 mg mL^{-1} by ultrasonic.

Synthesis of sulfur@GO composite: Na_2S and metallic sulfur were mixed and grinded in agate mortar, then the mixtures were quickly dissolved in DDI water and an orange solution was obtained easily. Followed, 10 mL of 1 wt% Triton X-100 (TX-100) (Biosharp, Korea) was added to the solution and kept stirring for 2 h 5 mL concentrated hydrochloric acid was added dropwise with vigorous stirring and a yellow suspension formed slowly. After vigorous stirring for 2 h, the yellow suspension was moved into oil bath with 70 °C. Then 20 mL GO with concentration of 1 mg mL^{-1} was added with vigorous stirring and kept for 1 h. After that, the suspension was centrifuged and washed with water for several times. The precipitation was dried by lyophilization at 40 °C and a dark gray sulfur@graphene oxide (S@GO) composite was obtained.

To improve the conductivity of S@GO composite, hydrogen iodide was used as reductant for GO reduction to get S@rGO composite with ultrahigh conductivity. The obtained S@GO precipitation was dispersed in 50 mL of 2 M KI solution, then 5 mL HCl was added quickly. The system was sealed and kept for 1 h in dark room, then centrifugation again and washed with DDI water and ethanol to remove HI and I_2 completely. Finally, the precipitation was dried by lyophilization at 40 °C and a black S@rGO composite was obtained.

For comparison, GO sheet with the thickness of about 30 μm by coating GO solution on clear glass and dried at 40 °C for 48 h. Then the GO sheet also was reduced with the former process.

2.2. Structural analyses

The morphologies and microstructures of the resulting products were examined by powder X-ray diffraction (XRD) using an X-ray diffractometer (Rigaku DLMAX-2550 V) with Cu-Kα radiation ($l = 1.54056$ A) and by field-emission scanning electron microscopy (FESEM, JEOL JSM-6700F). The composition of the graphene-coated sulfur composite was analyzed via Vario EL-III elemental analyzer (Elementar, Germany). More detailed structural information on the graphene-coated composite was obtained by Raman spectra by a laser Raman spectrometer (Renishaw inVia plus) with a laser wavelength of 633 nm and a spot size of 0.5 mm. FT-IR spectrum was obtained by an infrared spectrometer (Shimadzu, UV-2501PC, Japan). The volume conductivity of the composites was estimated by four probes method via pressuring sheet and test on an electrochemical station (CHI 660D, USA).

2.3. Cells assemble and electrochemical measurements

The S@rGO cathodes were fabricated by coating a NMP-based slurry with a mixture of 80 wt% S-based active material, 10 wt% acetylene black, and 10 wt% PVDF on an aluminum foil current collector. CR2016 coin cells were assembled in an argon-filled glove

box with the S-based composites as cathode and lithium metal as the counter and reference electrode, respectively. The electrolyte was 1 M LiTFSI (99.95%; Novolyte Tech Ltd. SuZhuo, China) dissolved in a mixture of DOL–DME (1:1 by volume) including 1 M $LiNO_3$ as an additive. A microporous membrane (Celgard 2400) was used as the separator. The galvanostatic charge–discharge test was conducted at a voltage interval of 1.0–3.0 V using a CT2001A LAND Battery Testing System. Cyclic voltammetry measurements were also carried out with the 2016 coin cell at a scan rate of 0.1 mV s^{-1} by using a CHI660D electrochemical station (CHI, USA). In addition, ac impedance measurements (Solartron 1287 electrochemical interface +1255B frequency analyzer) were also performed with amplitude of 5 mV at the applied frequency range from 1 MHz to 10 mHz. All electrochemical data were obtained at 20 °C. The DC impedance of S@GO and S@rGO powders was obtained using Solartron 1287 electrochemical station by pressing powders at 15 MPa and test at in the range from their open circuit potential (OPV) to OPV + 0.01 V.

3. Results and discussion

As shown in Fig. 1, a simple reaction for preparation of elemental sulfur is occurred after HCl was added into the orange solution (Na_2S + S) with TX-100 as dispersion agent. Therefore, sulfur with homogenous dispersibility and uniform particles size of several micrometers was obtained. TX-100 also play a role of linker between GO and sulfur by PEG group and benzene to adsorb on sulfur and GO, respectively. KI was employed as reductant for GO to rGO and a core–shell structured S@rGO with improved electronic conductivity was synthesized easily.

We noted that several common reductants, such as hydrazine hydrate, amine and NaOH, is not suit for reducing the GO on the surface of S@GO because of their strong alkalinity, in which the chemical formed sulfur particles is ease to dissolve. We also noted that HI as a GO reductant was reported, and I^- ions cannot react with elemental sulfur [26,27]. So in this work, we selected I^- ions as new reductant for GO reduction on the surface of S@GO composite. For the storage difficulty of HI, here we used KI–HCl aqueous as a substitution. The rGO coating layer with high conductivity was obtained after hydrogen iodide reduced GO in dark room during short time reaction. The mixture suspension changed from colorless to brown quickly, which means that I^- was oxidized to iodine (I_2). Possible reaction mechanism of GO reduction by HI was suggested in Fig. 1 [27]. For epoxy group, a ring-opening reaction will occur in hydrohalic acid solution. For –OH group, a nucleophilic substitution reaction will occur and the substituted iodide atoms are expected to be easily eliminated from the carbon lattice. Therefore, the rGO was recoverable and a graphene layer with more improved electronic conductivity obtained.

The conductivity of graphene is an important factor for electron transfer, especially for the insulator of sulfur active material. Here, we also compared the conductivity change of GO before and after HI reduction, and the similar result is obtained. The color of GO sheet (dried at 40 °C) changed from dark brown to black with metallic luster and the thickness also decreased from 30 μm to 12 μm. The conductivity of GO sheet is 1.4 MΩ and enhanced to 65 Ω after it was reduced by HI. The volume conductivity of S@GO and S@rGO were estimated by pressuring these composite to sheet with fixed diameter and measure the conductivity by linear scan in the range from open circuit potential (OPV) to 0.01 V + OPV (Fig. 2). It is obvious that all the two curves are approximately linear and the conductivity of S@GO without HI reduction is about 3 MΩ. While for the S@rGO by HI reduction, the conductivity enhanced miraculously to 73 Ω. This enhanced conductivity is attributed to that of the strong reducibility of HI at room temperature. Similar phenomenon is also observed on HI reduced pure GO membrane. From the color of S@rGO–HI reduction and S@GO we also can obviously find that HI can easily react with GO and the color changed from

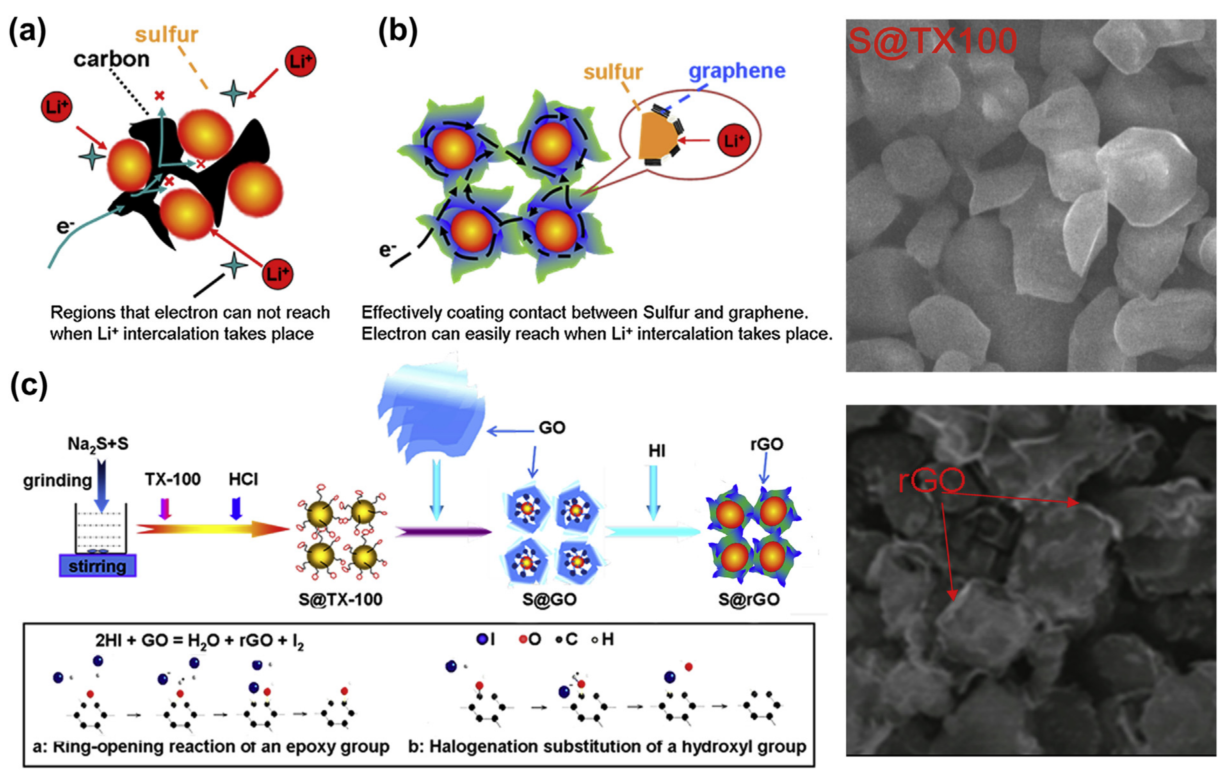

Fig. 1. Scheme of synthesizing S@rGO composite and possible reaction mechanism of GO reduction by hydrogen iodide.

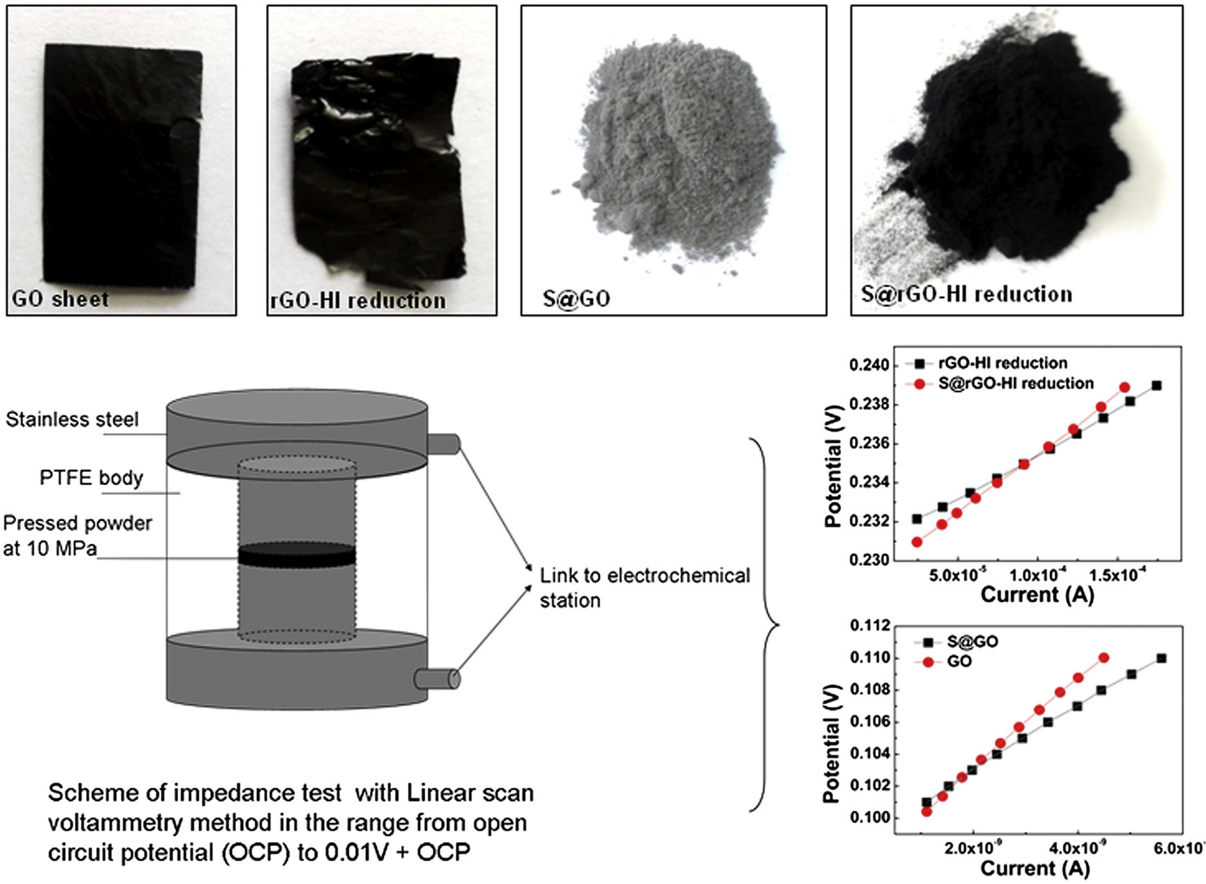

Fig. 2. Digital pictures of GO sheet, GO sheet after HI reduction, S@rGO–HI reduction and S@GO (up). Conductivity of GO, rGO–HI, S@GO and S@rGO–HI reduction obtained after pressing powder at 15 MPa (down).

gray to black. Also, we observe a phenomenon that GO shrinked after HI reduction, which indicated more tighter rGO layer formed and effect interact between S and rGO. These results confirmed that HI reduction is an effective method to improve the conductivity of GO-based electrode materials. According to the precious experiences, rGO will improve the electron transfer of electrochemical reaction, therefore, the dynamic performance are forecasted to improve.

The existence of TX-100 in the synthesized S@GO and S@rGO composites also was studied by FT-IR spectrum. As shown in Fig. 3,

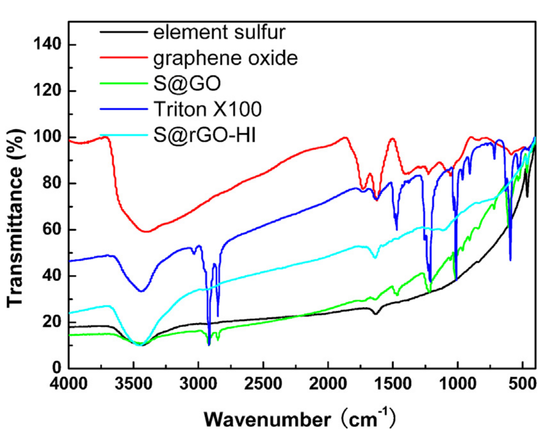

Fig. 3. FTIR spectrum of S@GO, S@rGO–HI, elemental sulfur, TX-100 and graphene oxide synthesized by modified Hummers method.

obvious adsorbed peaks at 670 cm^{-1}, 1050 cm^{-1}, 1498 cm^{-1}, 1859 cm^{-1} and 1921 cm^{-1} were observed, which are attributed to that of pure TX-100, indicating the existence of TX-100 as impurity in S@GO. In case of S@rGO, only the adsorbed peak of element sulfur was observed, and the typical adsorbed peak of TX-100 in S@GO disappeared, indicating an obvious difference after HI reduction and part of TX-100 as impurity is removed.

To obtain accurate electrochemical performance, the capacity of cells was evaluated according to the content of sulfur. As evidenced by elemental analyzer, high sulfur content of about 79.8% and 85.4% in S@GO and S@rGO, respectively, which is relatively higher sulfur content than most reports. High sulfur loading is attributed to that of our synthesis method, in which the weight ratio of sulfur to rGO can be modified easily. Minor difference of sulfur content between S@GO and S@rGO is attributed to that of the C=O, C–OH and COOH groups, which is reduced by HI and the carbon content decreased. This result indirectly confirmed that HI as reductant can reduce GO to rGO easily.

SEM images were supplied to study the coating layer of graphene on the surface of sulfur. As shown in Fig. 4, the pure GO and rGO (HI reduction) (a and a′) were 2D sheet structure with amount of crinkles. The length and width of GO is more than 1 μm and such a size level suits it for coating on the surface of micrometer sized sulfur. From low resolution images of S@GO and S@rGO (b′ and c′) we find that the composites with particle size of about 1–2 μm are very homogenous and no obvious aggregation was found. The high resolution images (b and c) also confirmed that GO and rGO successfully coated on the surface of sulfur. Obvious white stretch sheet structure of reduced graphene still was kept, which is clear

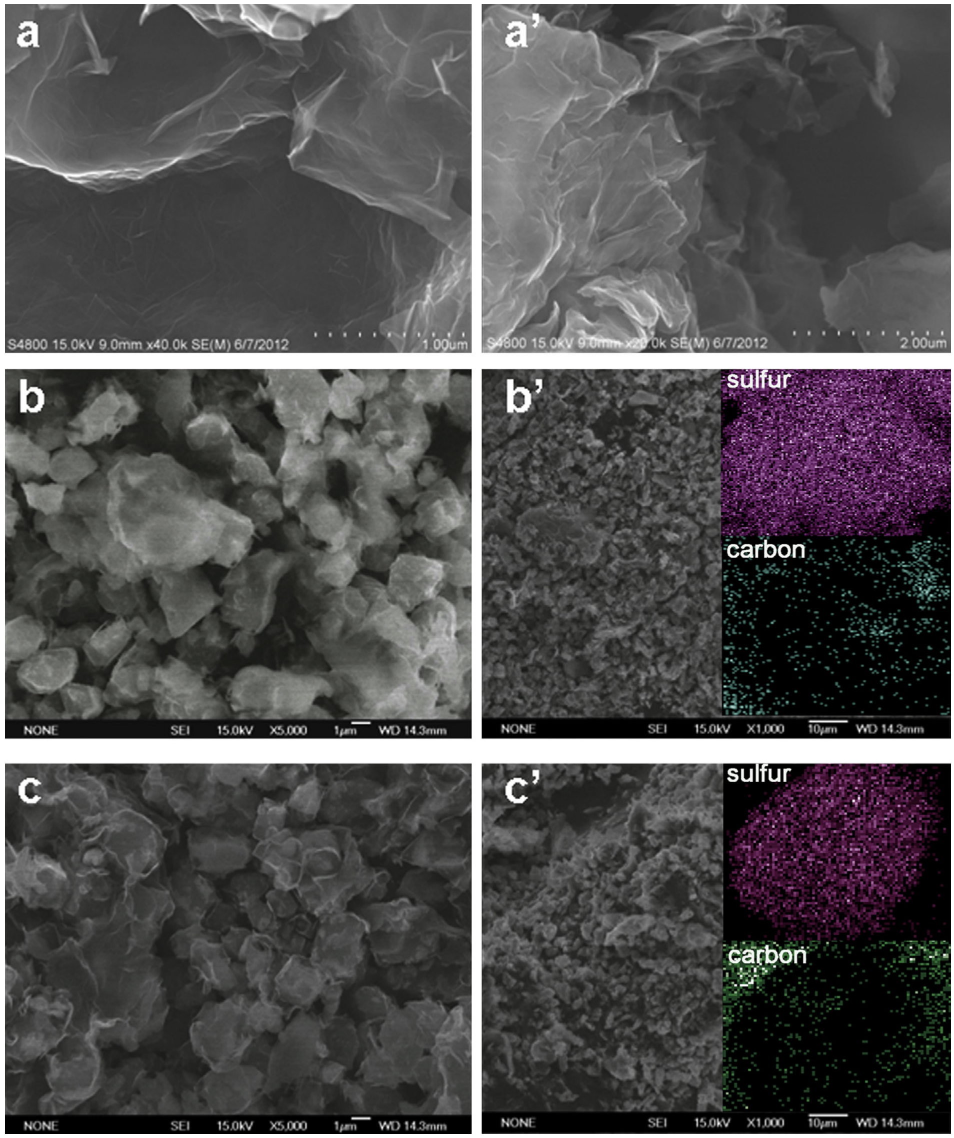

Fig. 4. SEM images of GO (a), pure rGO reduced by HI (a′), Sulfur@GO (b, b′) and Sulfur@rGO (c,c′) composites. The insert is sulfur and carbon mapping in an intact S@GO and S@rGO particle, respectively.

than that of graphene oxide for its higher conductivity. The homogenous particle size of the composites and perfect coating layer of graphene is attributed to that of TX-100, which not only effectively control the particle size of sulfur and the aggregation is prevented, but also play a role of linker between sulfur and graphene in the synthesis of S@GO. The sulfur and carbon mapping in an intact S@GO and S@rGO particle showed an obvious boundary between sulfur and graphene, which confirmed that a perfect coating layer of GO and rGO on the surface of elemental sulfur.

In Fig. 5a, XRD patterns of rGO obtained after HI reduction for several minutes show obvious difference compared with that of GO. The wide and flat diffraction peak of rGO membrane at about 24° is corresponding to the (0002) spacing of the graphene stacks, while the diffraction peak of GO centered at 10.3° corresponds to an increasing interplanar distance due to the existence of oxygen functional groups and some other structural defects, which are corresponding to most literature [15–17,24,28]. Elemental sulfur was obtained by chemical reaction-deposition method successfully and the sulfur particles diffraction peaks in S@GO and S@rGO are accordance to that of standard PDF card (00-008-02475). The strongest diffraction peak at 23.07° is attributed to the (222) peak of orthorhombic sulfur. The primary particle size of sulfur estimated by Scherrer equation is about 30 nm. No obvious diffraction peak of GO or rGO was found for its low content in the S@GO and S@rGO composites.

The structure change, which affect the conductivity recovery degree of rGO after HI reduction was evaluate by Raman spectrum. As shown in Fig. 5b, the basic features of the sulfur spectrum at low Raman shift in terms of the assignments of Scott, McCullough, and Kruse [29] for the Raman-active $2A_1 + 3E_2 + 2E_3$ species appropriate to molecular unit S_8 of D_{4d} symmetry. The peaks centered at 84 and 151 cm^{-1} are assigned to the E_2 symmetry species; those at 218 and 474 cm^{-1} are assigned to the A_1 species; and those at 248 and 437 cm^{-1} are assigned to the E_3 species. According to the assignments of Scott et al., the remaining E_2 mode is accidentally degenerate with the A_1 mode at 475 cm^{-1}. The peak centered at 188 cm^{-1} is presumably the Raman-forbidden B1 fundamental appearing in violation of strict D_{4d} selection rules. The peak at 1336 cm^{-1} and 1591 cm^{-1} is accordance to that of D band and G band of graphite, respectively. The integral area ratio of D band to G

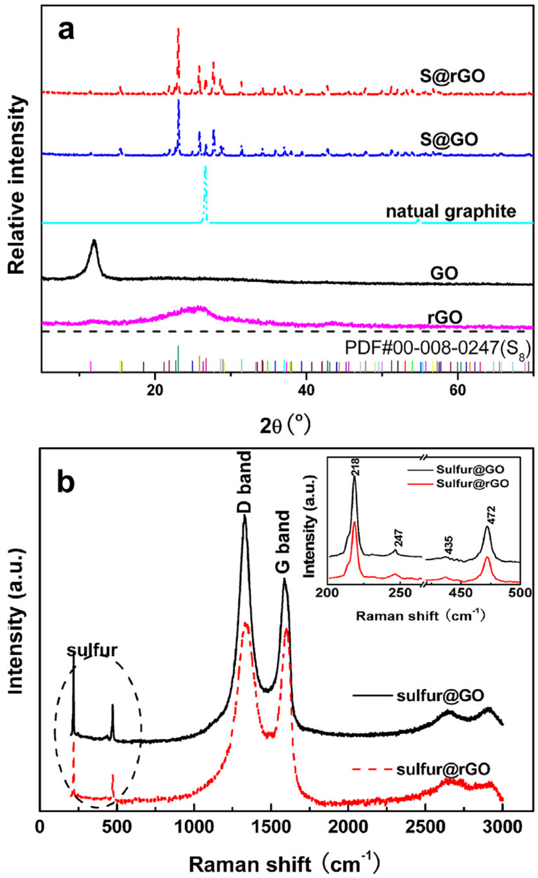

Fig. 5. XRD patterns (a) and Raman spectrum (b) of GO, rGO, S@GO and S@rGO, the insert is the magnification of sulfur spectrum.

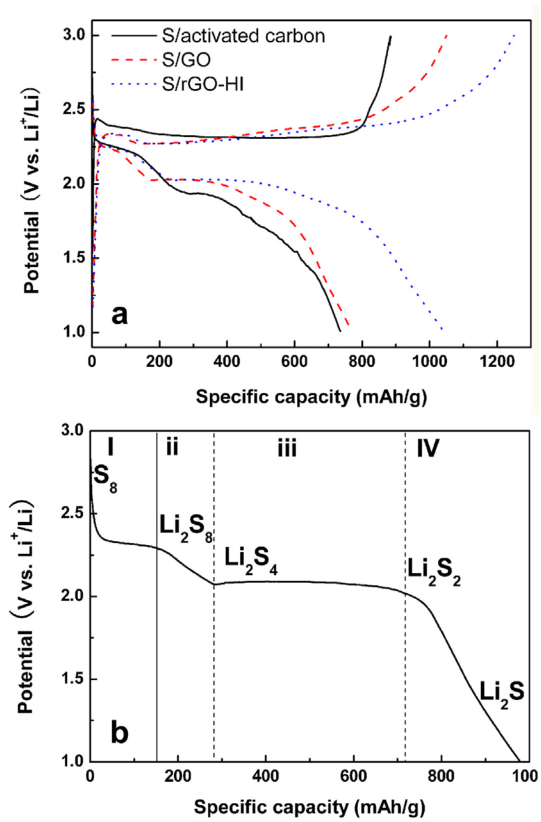

Fig. 6. Voltage profile of the first charge/discharge of batteries, recorded at 0.05C (a). The lithium insertion in sulfur at different status (b). 1C = 1675 mA g^{-1}. The capacity is calculated by the sulfur loading.

band of S@rGO, which represents the carbon hybridization of sp2 and sp3, became smaller than that of S@GO, indicating a conductivity recovery of graphene after HI reduction.

The electrochemical performance of the as assembled single cell was shown in Fig. 6a. With HI as reduced agent of GO, the S@rGO-HI electrode showed charge/discharge capacity of 1210 mAh g^{-1} and 1040 mAh g^{-1}, respectively. While for the S@GO electrode, only about 775 mAh g^{-1} discharge capacity was obtained. The similar phenomenon is that after charge potential raised to 2.45 V, the potential can not keep a stable value but an obvious descend. Then the charge platform formed with slowly decline, according to the complicated electrochemical reaction and the shuttle effect of polysulfide ion in Li/S cell, which can be found in most of Li–S batteries. Fig. 6b depicts the voltage profile of the discharge of a high sulfur loading Li/S cell (The capacity values in this article are calculated according to the mass of S). From the viewpoint of phase transitions, the discharge of sulfur can be divided into four regions (Fig. 6b). In these regions, the process (Region ii) is more complicated than all others because it is affected by the chemical equilibriums between each type of lithium polysulfides species and the solubility of lithium polysulfides in the electrolyte. Due to the non-conductive nature of Li_2S_2 and Li_2S, region IV is kinetically slow and normally suffers high polarization. According to the reported mechanisms for oxidation and reduction of sulfur during discharge/charge process, the plateaus at around 2.35 V can be assigned to the reduction of elemental S to Li_2S_8 (Region i). The plateau at about 2.1 V is related to the reduction of Li_2S_4 to Li_2S_2 (Region iii). Besides, one obvious slope is observed in the range of 2.3 V–2.1 V, which is attributed to the reduction of Li_2S_8 to Li_2S_4 (Region ii). Another slope in the range of 2.1 V to 1.0 V is complicated because of the dissolved Li_2S_4 can be reduced to Li_2S_2 (insoluble) and Li_2S (insoluble) simultaneously (Region IV). This is accordance to that of most cases, in which the final discharge products are a mixture of Li_2S_2 and Li_2S [9,11,15,30,31].

To verify the charge/discharge mechanism, CV technique was used to study the oxidation/reduction behavior during the charge/discharge process. As shown in Fig. 7, two reduced peaks and one oxidation peak was observed, respectively, which is accordance to that of charge/discharge profile (Fig. 6). It should be noted that the oxidation peak seems to be a lap of two peaks, which is attributed to the mixed reaction among Li_2S_n ($1 \leq n \leq 4$). The integral area of oxidation and reduced peak of S@rGO is larger than that of S@GO, indicating larger electric capacitance. The anodic peak potential of these two cells is approximate, which confirmed that the lithium ion insertion mechanism is similar. The cathodic peak potential of S@rGO–HI electrode is somewhat higher than that S@GO, indicating a slight polarization due to different electrode structure. We cannot distinguish the reduction peaks occurred in the (Region ii) and (Region IV) processes, because of the lap of reactions in this voltage range and their delithiation potentials are mixed.

The Nyquist plots of different electrode obtained under various open-circuit potential are shown in Fig. 7b. Only one semicircle and one straight line can be seen in each Nyquist plot because the solid electrolyte interface (SEI) has not been formed in the initial charge cycle. The semicircle with a high frequency intercept on the R_s reveals the cell resistance (of the electrolyte and electrode) of about 5 Ω, while the semicircle itself elucidates the characteristic of the charge transfer resistance (R_{ct}) between the electrolyte and the active material sulfur-based composites. A very low frequency

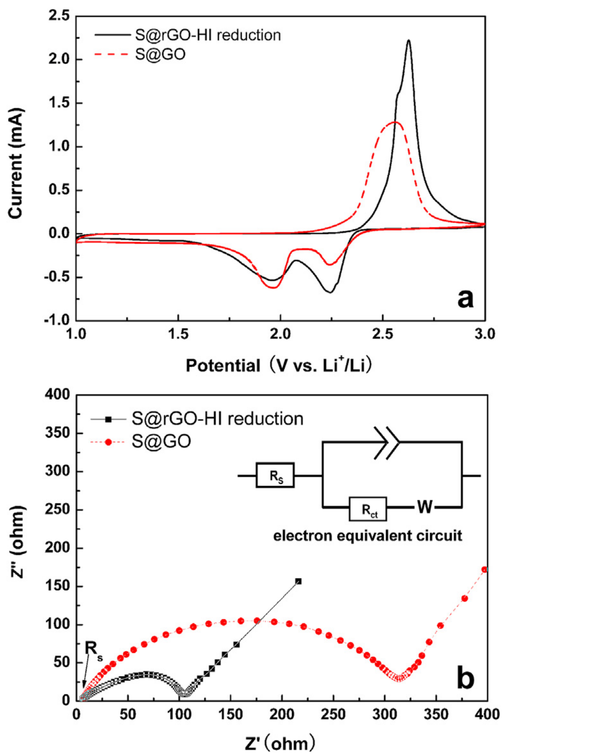

Fig. 7. CV (a) and AC impedance (b) of S@GO and S@rGO electrodes, the insert is the electron equivalent circuit.

region of the straight line observed is attributed to the diffusion of the Li ions into the particles of sulfur-based composites or the so-called Warburg diffusion. The R_{ct} resistance of S@rGO is about 110 Ω, only about 30% of S@GO, which confirmed that the electron resistance marvelously descends by HI reduction.

To alleviate the shuttle of polysulfide ions during the charge/discharge process, we tried to electrochemically activate the electrode in the initial several charge/discharge cycles at high current density of 1 C (Fig. 8 left). Obviously, after initial discharge process of the as assembled battery, the initial charge process with a small current density (as shown in Fig. 8 left, 0.05 C initial charge/discharge) is difficultly finished. A long time charge plateau at about 2.4 V and large irreversible charge capacity (3700 mAh g^{-1}) showed which is inconsistent with the theoretical capacity of sulfur. Serious polarization and irreversible capacity for the unstable electrochemical status of as assembled batteries maybe attribute to the reaction on the surface of anode. As shown in Fig. 8 (right), this time-consuming charge process in the first charge process maybe relate to several factors, including impurities oxidation, shuttle effect of polysulfide on anode, and the unstable electrode surface at initial status. In these factors, the competitive reaction among the deposited Li_2S_x, formed sulfur and lithium metal on the anode and unstable electrode surface should be the most important factor (Fig. 8 right). The content of lithium polysulfide on the surface of Li foil is related to the initial discharge/charge time. In the initial charge process, the deposited lithium polysulfide will be reduced to Li metal and the released polysulfide anion (S_x^{2-}) will react again with lithium to form Li_2S_x. These two completive reactions cause serious polarization of battery and a number of charges consumed. Therefore, an initial time-consuming charge plateau characteristic was observed at small current density before stable SEI membrane formed on Li foil. After four cycles of rapid electrochemical activation at 1C, the shuttle effect of polysulfide anions miraculously disappeared, even at a low current density of 0.05 C. This obvious improvement is attributed to the rapid phase transfer between elemental sulfur and lithium sulfide in initial several cycles of charge/discharge process, and the number of soluble polysulfide ions (S_8^{2-} and S_4^{2-}) deposited on anode decrease in shorter time. In addition, fast formation of SEI membrane on Li foil also is advantage to prevent the deposition of polysulfide. Thus, a more stable electrode structure fast formed in short-time electrochemical activation. The rapid electrochemical activation should be an effective method for electrode structure optimization and alleviate the shuttle of sulfur in the initial charge/discharge process.

The cycling performance of S-based electrodes was evaluated by 200 cycles charge/discharge process. As shown in Fig. 9, the discharge capacity of S@GO remained about 480 mAh g^{-1} after 200 cycles with 0.05 C discharge, and the capacity decay ratio is about 48%. The S@rGO electrode delivers about 980 mAh g^{-1} of discharge capacity, and the decay ratio obviously decreases to 18%. The higher capacity retention ratio of S@rGO is attributed to that of the existence of HI reduced rGO layer, which does not easy dissolve in the DOL-DME solvent, and its high conductivity is advantage to improve the electron transfer. Moreover, 570 mAh g^{-1} of discharge capacity retained on 1 C rate, which indicated improved high C-rate performance.

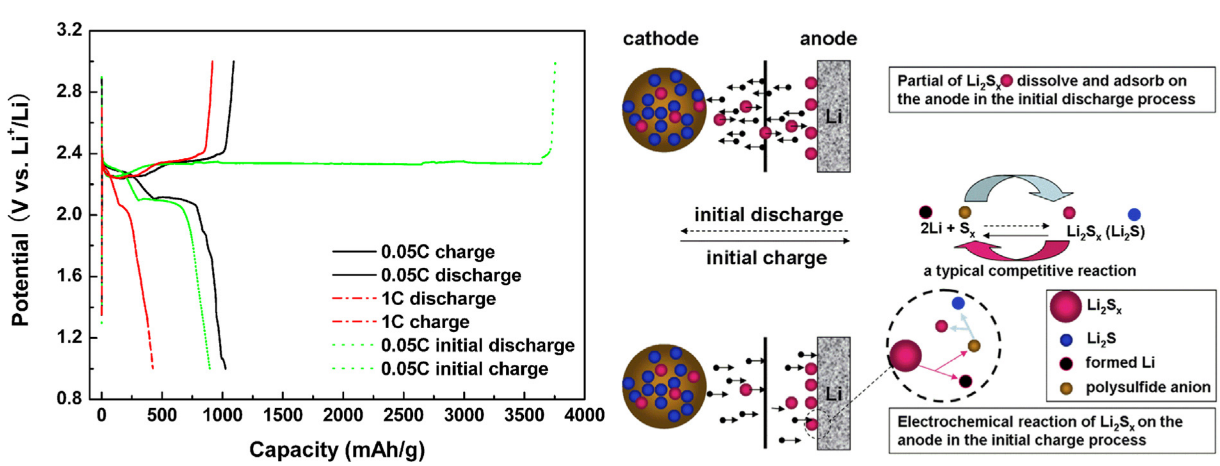

Fig. 8. Electrochemistry performance of S@rGO before and after high current density rate (1C) activation for four cycles (left); Scheme of electrochemical competitive reaction between Li_2S_x and sulfur + Lithium on the surface of anode (right).

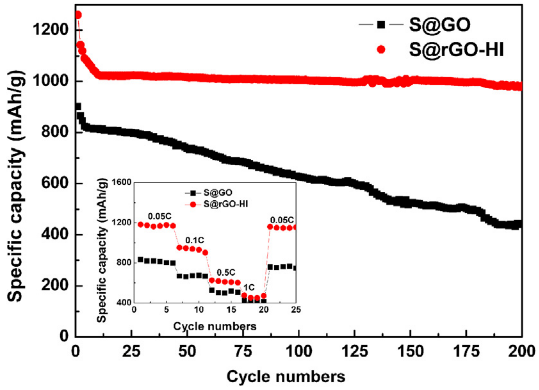

Fig. 9. Electrochemical performance of S@GO and S@rGO electrodes, a: cycling performance at 0.05C, b: C-rate performance.

The rGO by HI reduction clearly performs very well as a means to stabilize the S electrode. The role of HI was significant to prevent the shuttle of polysulfides between electrodes. With HI as reduction agent, the group such as C=O, C–OH and COOH was removed. Therefore, the dissolution of GO in organic agents (DME and DOL) was prevented effectively, this has been confirmed by simple dissolving several microgram of GO and rGO in the electrolyte and observes the color change of the agent. Besides, as a carbon conducting layer, rGO is plastic and this can effectively delay the diffusion of polysulfides and the collapse of rGO layer after lithium insertion and volume expansion.

4. Conclusion

A novel chemical approach is used to synthesize an S@rGO composite by HI reduced graphene sheet wrapping on the surface of sulfur and its electrochemical performance as cathode of lithium rechargeable batteries was studied. The S@rGO composite cathode with high sulfur content of about 85% display good reversibility, excellent capacity stability of about 980 mAh g^{-1} (0.05 C) up to 200 cycles of charge/discharge. The unique graphene coating layer and the good conductivity of graphene obtained by HI reduction contributes to the good cycling stability. The rGO layer also accommodates the volume change of the electrode during the Li–S electrochemical reaction and the shuttle of polysulfide in the electrolyte. This research demonstrates a new approach to improve the application of graphene as conducting material or modification material in designing other electrode materials.

Acknowledgment

This work is financially supported by Leading Academic Discipline Project of Shanghai Municipal Education Commission (No. J50102), the National Natural Science Foundation of China (Grant No. 61071040), Innovation Fund of Shanghai University (A.10-0101-11-008), Shanghai College Student Research Fund and Shanghai University Teacher Indurstry-University-Research Cooperation Project. We also thank the Analysis and Research Center of Shanghai University for sample characterization.

References

[1] A. Kraytsberg, Y. Ein-Eli, Advanced Energy Materials 2 (2012) 922–939.
[2] Z.-D. Yao, W. Wei, J.-L. Wang, J. Yang, Y.-N. Nuli, Acta Physico-Chimica Sinica 27 (2011) 1005–1016.
[3] V.S. Kolosnitsyn, E.V. Karaseva, Russian Journal of Electrochemistry 44 (2008) 506–509.
[4] C. Barchasz, F. Molton, C. Duboc, J.-C. Lepretre, S. Patoux, F. Alloin, Analytical Chemistry 84 (2012) 3973–3980.
[5] R. Elazari, G. Salitra, A. Garsuch, A. Panchenko, D. Aurbach, Advanced Materials 23 (2011) 5641–5644.
[6] J. Xiulei, L. Kyu Tae, L.F. Nazar, Nature Materials 8 (2009) 500–506.
[7] G. He, X. Ji, L. Nazar, Energy & Environmental Science 4 (2011) 2878–2883.
[8] C. Liang, N.J. Dudney, J.Y. Howe, Chemistry of Materials 21 (2009) 4724–4730.
[9] M. Rao, W. Li, E.J. Cairns, Electrochemistry Communications 17 (2012) 1–5.
[10] W. Ahn, K.-B. Kim, K.-N. Jung, K.-H. Shin, C.-S. Jin, Journal of Power Sources 202 (2012) 394–399.
[11] S. Doerfler, M. Hagen, H. Althues, J. Tuebke, S. Kaskel, M.J. Hoffmann, Chemical Communications 48 (2012) 4097–4099.
[12] X. Liang, Z. Wen, Y. Liu, H. Zhang, J. Jin, M. Wu, X. Wu, Journal of Power Sources 206 (2012) 409–413.
[13] W. Choi, I. Lahiri, R. Seelaboyina, Y.S. Kang, Critical Reviews in Solid State and Materials Sciences 35 (2010) 52–71.
[14] M. Rao, X. Geng, X. Li, S. Hu, W. Li, Journal of Power Sources 212 (2012) 179–185.
[15] J.-Z. Wang, L. Lu, M. Choucair, J.A. Stride, X. Xu, H.-K. Liu, Journal of Power Sources 196 (2011) 7030–7034.
[16] F. Zhang, Y. Dong, Y. Huang, G. Huang, X. Zhang, L. Wang, Journal of Physics Conference Series 339 (2012) 012003.
[17] X. Liang, Y. Liu, Z. Wen, L. Huang, X. Wang, H. Zhang, Journal of Power Sources 196 (2011) 6951–6955.
[18] M.-S. Park, J.-S. Yu, K.J. Kim, G. Jeong, J.-H. Kim, Y.-N. Jo, U. Hwang, S. Kang, T. Woo, Y.-J. Kim, Physical Chemistry Chemical Physics 14 (2012) 6796–6804.
[19] Y. Fu, A. Manthiram, Journal of Physical Chemistry C 116 (2012) 8910–8915.
[20] S. Mingming, Z. Shichao, J. Tao, Z. Lan, Y. Jinhua, Electrochemistry Communications 10 (2008) 1819–1822.
[21] Z. Shi-chao, Z. Lan, W. Wei-kun, X. Wen-juan, Synthetic Metals 160 (2010) 2041–2044.
[22] L. Yin, J. Wang, F. Lin, J. Yang, Y. Nuli, Energy & Environmental Science 5 (2012) 6966–6972.
[23] L. Yin, J. Wang, X. Yu, C.W. Monroe, Y. NuLi, J. Yang, Chemical Communications 48 (2012) 7868–7870.
[24] F.Y. Ban, S.R. Majid, N.M. Huang, H.N. Lim, International Journal of Electrochemical Science 7 (2012) 4345–4351.
[25] O.O. Kapitanova, G.N. Panin, A.N. Baranov, T.W. Kang, Journal of the Korean Physical Society 60 (2012) 1789–1793.
[26] C. Wu, X. Huang, G. Wang, L. Lv, G. Chen, G. Li, P. Jiang, Advanced Functional Materials (2012) 506–513.
[27] S. Pei, J. Zhao, J. Du, W. Ren, H.-M. Cheng, Carbon 48 (2010) 4466–4474.
[28] M.J. McAllister, J.-L. Li, D.H. Adamson, H.C. Schniepp, A.A. Abdala, J. Liu, M. Herrera-Alonso, D.L. Milius, R. Car, R.K. Prud'homme, I.A. Aksay, Chemistry of Materials 19 (2007) 4396–4404.
[29] A.T. Ward, The Journal of Physical Chemistry 72 (1968) 4133–4139.
[30] L. Ji, M. Rao, H. Zheng, L. Zhang, Y. Li, W. Duan, J. Guo, E.J. Cairns, Y. Zhang, Journal of the American Chemical Society 133 (2011) 18522–18525.
[31] Y.-J. Choi, Y.-D. Chung, C.-Y. Baek, K.-W. Kim, H.-J. Ahn, J.-H. Ahn, Journal of Power Sources 184 (2008) 548–552.